Electronic-to-Vibrational Energy Transfer from $I^*(5\,^2P_{1/2})$ to $I_2(25<v<43)$

G. E. Hall, W. J. Marinelli, and P. L. Houston*

Department of Chemistry, Cornell University, Ithaca, New York 14853 (Received: November 16, 1982)

Electronic-to-vibrational energy transfer from $I^*(5\,^2P_{1/2})$ to $I_2(25<v<43)$ has been observed. I* was created by pulsed laser photolysis of either I_2/Ar mixtures at 475 nm or CF_3I/I_2/Ar mixtures at 266 nm, while the resulting vibrational distribution of I_2 was monitored by laser-induced fluorescence on the $I_2(B\leftarrow X)$ transition. The experimental results are consistent with a nascent I_2 product distribution which is inverted, with a substantial fraction of the I_2 molecules formed in $v > 30$. Roughly 2% of the I* deactivations result in $I_2(v=40)$. The rate constants for vibrational relaxation of $I_2(v=40)$ by argon, helium, and I_2 at room temperature are $(7.3 \pm 0.3) \times 10^5$ s^{-1} torr^{-1}, $(1.02 \pm 0.2) \times 10^6$ s^{-1} torr^{-1}, and $(1.8 \pm 0.4) \times 10^6$ s^{-1} torr^{-1}, respectively. These results have important implications for the mechanism of I_2 dissociation in the chemical oxygen/iodine laser. A chain-branching mechanism consisting of the steps $I^* + I_2 \rightarrow I + I_2(20<v<40)$, $I_2(20<v<40) + O_2(^1\Delta) \rightarrow 2I + O_2$, and $O_2(^1\Delta) + I \rightarrow O_2 + I^*$ may be responsible for the dissociation.

I. Introduction

Electronic-to-vibrational (E → V) energy transfer has been the subject of intensive experimental and theoretical investigation. The study of these reactions is important to an understanding of the chemistry of the upper atmosphere, to the development of new laser systems which employ either E → V or V → E pumping mechanisms, and to the prediction of the direction and efficiency of photochemical reactions.

In a recent review[1] of electronic energy transfer from excited halogen atoms ($I^*(5^2P_{1/2})$; $Br^*(4^2P_{1/2})$) it has been demonstrated that a minimal energy defect, ΔE, and a small change in vibrational quantum number, Δv, are important in maximizing the total rate of E → V transfer, although these factors make little difference in determining the total amount of energy transferred per collision. The transfer of electronic energy from I* to I_2

$$I^*(7603\ \text{cm}^{-1}) + I_2 \rightarrow I + I_2(v<40) \quad (1)$$

is especially interesting from this point of view in that the dense vibrational and rotational manifolds of I_2 minimize ΔE but require a large Δv.

Our initial work on this reaction was prompted by an interest in the kinetic mechanism of the chemical oxygen/iodine laser. Previous investigations of this system[2-10] had resulted in the following mechanism:

$$O_2(^1\Delta) + O_2(^1\Delta) \rightarrow O_2(^1\Sigma) + O_2(^3\Sigma) \quad (2)$$

$$O_2(^1\Delta) + I^* \rightarrow O_2(^1\Sigma) + I \quad (3)$$

$$O_2(^1\Sigma) + I_2 \rightarrow O_2(^1\Sigma) + 2I \quad (4)$$

$$O_2(^1\Delta) + I \rightarrow O_2(^3\Sigma) + I^* \quad (5)$$

$$I^* \rightarrow I + h\nu\ (7603\ \text{cm}^{-1}) \quad (6)$$

Reactions 2–4 provide a mechanism for producing and maintaining dissociation of I_2, while reactions 5 and 6 invert the iodine atom population, allowing laser emission at 1.315 μm. Although steps 5 and 6 seem well-established, recent investigations from both our laboratory[11,12] and that of Heidner et al.[13] have cast doubt on the efficiency of reactions 2–4 in dissociating I_2.

A possible chain mechanism for I_2 dissociation in this system involves the initial creation of I* via reactions 2–5 followed by the steps

$$I^* + I_2 \rightarrow I + I_2(20<v<45) \quad (1b)$$

and

$$I^* + I_2(20<v<45) \rightarrow 3I \quad (7a)$$

or

$$O_2(^1\Delta) + I_2(20<v<45) \rightarrow O_2 + 2I \quad (7b)$$

The total rate of deactivation of I* by I_2 has been measured several times;[14-22] the most recent values center around 1.2

(1) P. L. Houston, "Photoselective Chemistry", Part 2, J. Jortner, Ed., Wiley-Interscience, New York, 1981, p 381.
(2) S. J. Arnold, N. Finlayson, and E. A. Ogryzlo, *J. Chem. Phys.*, **44**, 2529 (1966).
(3) R. G. Derwent and B. A. Thrush, *Chem. Phys. Lett.*, **9**, 591 (1971).
(4) R. G. Derwent and B. A. Thrush, *J. Chem. Soc., Faraday Trans. 2*, **68**, 720 (1972).
(5) R. G. Derwent and B. A. Thrush, *Trans. Faraday Soc.*, **53**, 162 (1972).
(6) R. G. Derwent and B. A. Thrush, *Trans. Faraday Soc.*, **67**, 2036 (1971).
(7) R. G. Derwent, D. R. Kearns, and B. A. Thrush, *Chem. Phys. Lett.*, **6**, 115 (1970).
(8) A. T. Pritt, Jr., R. D. Coombe, D. Pilipovich, R. E. Wagner, D. Benard, and C. Dymek, *Appl. Phys. Lett.*, **31**, 745 (1977).
(9) W. E. McDermott, N. R. Pchelkin, D. J. Benard, and R. R. Bousek, *Appl. Phys. Lett.*, **32**, 469 (1978).
(10) R. J. Richardson and C. E. Wiswell, *Appl. Phys. Lett.*, **35**, 138 (1979).
(11) R. G. Aviles, D. R. Muller, and P. L. Houston, *Appl. Phys. Lett.*, **37**, 358 (1980).
(12) D. F. Muller, R. H. Young, P. L. Houston, and J. R. Wiesenfeld, *Appl. Phys. Lett.*, **38**, 404 (1981).
(13) R. F. Heidner III, C. E. Gardner, T. M. El-Sayed, and G. I. Segal, *Chem. Phys. Lett.*, **81**, 142 (1981); R. F. Heidner III, C. E. Gardner, T. M. El-Sayed, and G. I. Segal, private communication.
(14) R. J. Donovan and D. Husain, *Nature (London)*, **206**, 171 (1965).
(15) A. B. Callear and J. F. Wilson, *Trans. Faraday Soc.*, **63**, 1358 (1967).
(16) A. B. Callear and J. F. Wilson, *Trans. Faraday Soc.*, **63**, 1983 (1972).
(17) J. J. Deakin and D. Husain, *J. Chem. Soc., Faraday Trans. 2*, **68**, 603 (1972).
(18) D. H. Burde, R. A. McFarlane, and J. R. Wiesenfeld, *Chem. Phys. Lett.*, **32**, 296 (1975).
(19) D. H. Burde and R. A. McFarlane, *J. Chem. Phys.*, **64**, 1850 (1976).
(20) I. Arnold, F. J. Comes, and S. Pionteck, *Chem. Phys.*, **9**, 237 (1975).

0022-3654/83/2087-2153$01.50/0

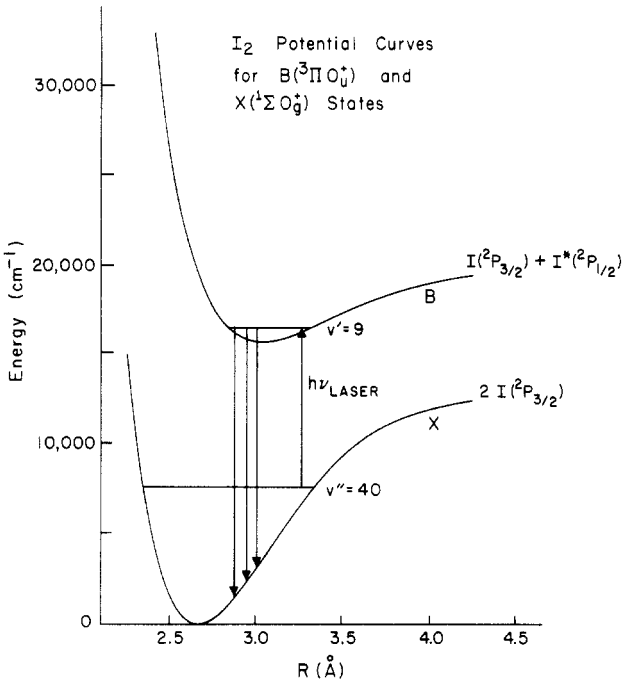

Figure 1. Laser-induced fluorescence detection scheme for vibrationally hot $I_2(X)$. A tunable near-infrared laser excited high vibrational levels of $I_2(X)$ to the B state, and blue-shifted fluorescence was collected.

$\times 10^6$ s^{-1} $torr^{-1}$. Our study investigates what fraction of that rate produces I_2 in a vibrationally excited state (i.e., reaction 1) and measures the rates of vibrational deactivation of $I_2(v=40)$ by I_2, Ar, and He. It is found that about 2% of the I* deactivations by I_2 leave I_2 in $v = 40$ and that the vibrational relaxation rates for $I_2(v=40)$ are $(1.8 \pm 0.4) \times 10^6$, $(0.73 \pm 0.03) \times 10^6$, and $(1.0 \pm 0.2) \times 10^6$ s^{-1} $torr^{-1}$ for deactivation by I_2, Ar, and He, respectively.

II. Experimental Section

These experiments use the photolysis of precursors (CF_3I or I_2) to produce I* in I_2/Ar or I_2/He mixtures. Anti-Stokes laser-induced fluorescence (LIF) of I_2 on the B–X transition (see potential diagram, Figure 1) was used to observe the vibrational population distribution in the X state following transfer of energy from I* to I_2. The I_2(B–X) transition has been studied extensively, and the details of the spectrum need not be reviewed here. The quantum yields of I* from photolysis of CF_3I in the A band[23] and I_2 in the B–X transition[24] are well-known. Trifluoromethyl iodide was chosen as an I* precursor because it is an inefficient quencher of I* ($k < 6.6 \times 10^{-2}$ s^{-1} $torr^{-1}$), and because the primary fate of the CF_3 fragment in this system is recombination with I atoms ($k = 5.0 \times 10^5$ s^{-1} $torr^{-1}$).[25]

A. Apparatus. A schematic diagram of the experimental apparatus is shown in Figure 2. The fluorescence cell, constructed of Pyrex and externally blackened, was 65 cm long, 3.8 cm in diameter, and equipped with Brewster angle windows and Wood's horns at each end to reduce scattered light from window reflections. A Pyrex window, centrally located along the cell axis, was used to view

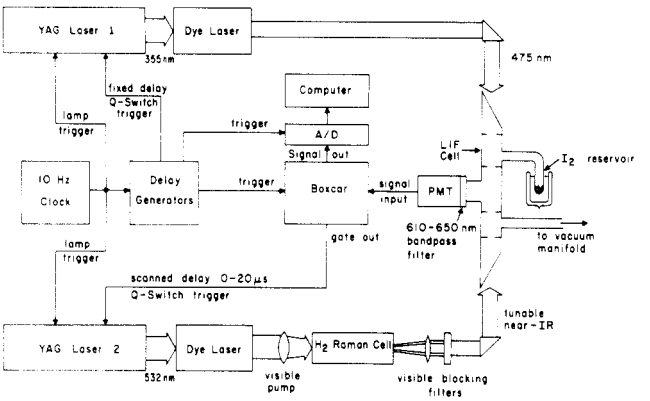

Figure 2. Schematic diagram of experimental apparatus. See text for details.

fluorescence at right angles to the counterpropagating photolysis and probe laser beams. Arrays of black anodized aluminum baffles, placed in each arm of the cell, acted to further reduce scattered laser radiation. The cell was connected to a standard vacuum manifold through which all components could be independently introduced. Their pressures were measured with a capacitance manometer (MKS-221HS-10).

The in situ production of I* from the CF_3I precursor was accomplished via photolysis at 266 nm by a Nd:YAG laser (Quanta-Ray, DCR-1). Typical fluences of 2–4 mJ/cm^2 were employed which, using absorption cross sections of Dacey,[28] resulted in I* concentrations of $(0.7–1.4) \times 10^{-1}$ mtorr per pulse. A smaller amount of I* was also produced from photolysis of I_2 at this wavelength, as was previously noted by Clear and Wilson.[29] Due to this multiple photolysis problem, experiments done to quantify the efficiency of the transfer process were performed on I_2/Ar mixtures by using photolysis of I_2 at 475 nm by an excimer pumped dye laser (Lambda-Physik EMG-101/FL2002). Typically, fluences and I_2 concentrations were chosen such that initial I* concentrations were comparable with those attained via 266-nm photolysis of CF_3I.

Vibrationally excited I_2 was detected by laser-induced fluorescence with a first Stokes (S_1) or second Stokes (S_2) Raman-shifted dye laser tuned to selected bands in the B–X transition. The dye laser (Nd:YAG, Quanta-Ray DCR-1A/PDL-1) was operated by using R590, R610, or DCM laser dyes, producing typical pulse energies of 30–70 mJ at 10 pps. The output from the dye laser was focused into an 86-cm long, hydrogen-filled, Raman shifter[26] by a 75-cm focal length lens. After passing through a series of filters to block the pump beam and any unwanted Stokes orders, the output from the Raman shifter was collimated by a 100-cm focal length quartz lens and directed through the fluorescence cell. A thermopile (Epply) was used to monitor the average power of the probe beam, and its output was used to normalize the observed fluorescence signal. Conversion of the pump beam on the H_2 Q(1) line at 4155.28 cm^{-1} was optimized for S_1 and S_2 at approximately 70 and 25 atm, respectively. Typical conversion efficiencies of 17% for S_1 and 6% for S_2 were obtained. The line width of the pump laser was typically 0.5 cm^{-1} with the Raman contribution to the line width less than 0.1 cm^{-1}.[27]

The I_2(B–X) visible fluorescence was viewed with a multi-alkali, red-sensitive photomultiplier (Hamamatsu

(21) Yu. Tolmachev and V. A. Kartazaev, *Opt. Spectrosk.*, **41**, 95 (1976).
(22) A. J. Grimley and P. L. Houston, *J. Chem. Phys.*, **68**, 3366 (1978).
(23) T. Donohue and J. R. Wiesenfeld, *J. Chem. Phys.*, **63**, 3130 (1975).
(24) D. H. Burde, R. A. McFarlane, and J. R. Wiesenfeld, *Phys. Rev. A*, **10**, 1917 (1974).
(25) G. N. Vinokurov and V. Yu. Zalesskii, *Sov. J. Quantum Electron.*, **8**, 1191 (1978).
(26) D. F. Muller, Ph.D. Thesis, Cornell University, 1981.
(27) D. F. Muller, R. H. Young, P. L. Houston, and J. R. Wiesenfeld, *Appl. Phys. Lett.*, **38**, 404 (1981).
(28) J. R. Dacey, *Discuss. Faraday Soc.*, **14**, 84 (1953).
(29) R. D. Clear and K. R. Wilson, *J. Mol. Spectrosc.*, **47**, 39 (1973).

R928). An infrared blocking filter (Schott, KG3) and various combinations of long and short wavelength pass interference and color filters were employed to reject scattered photolysis and probe laser radiation and to limit the bandwidth of the fluorescence seen by the photomultiplier. A boxcar signal averager (PAR Model 162) in conjunction with a computerized data acquisition system (DEC LPS11-1/LSI11/2 or 11/23) was used to record and store data for subsequent transfer to the Cornell Chemistry Computer Facility (PRIME 850) for analysis and plotting.

Two distinctly different types of experiments were performed with this apparatus. One type scanned the wavelength of the probe laser to establish the identity of the observed species as I_2 and to obtain its approximate vibrational distribution. The second type scanned the delay between the creation of I* and the subsequent probe of I_2 to obtain the kinetic behavior of any single vibrational level of the X state.

Experiments observing kinetics were performed with $CF_3I/I_2/Ar$ mixtures so that the concentrations of I* and I_2 could be varied independently at constant photolysis laser fluence. Typical scans covered a 15-μs delay range with an additional ≃4 μs of pretrigger. The scans were accomplished by taking advantage of the approximately 20-μs window over which the Nd:YAG laser Q-switch could be triggered without appreciable change in laser output energy. The flashlamps of both the photolysis and probe lasers were triggered simultaneously by a common pulse generator operating at 10 Hz. A series of additional simultaneous and delayed pulses triggered the A/D converters, oscilloscope, and boxcar, while a final delayed pulse triggered the photolysis laser Q-switch approximately 5 μs into the 20-μs scan range of the boxcar. The A channel gate out of the boxcar was amplified and used to trigger the probe laser Q-switch, and the B channel aperture was set to capture the fluorescence signal. The internal sweep generator of the boxcar was then used to scan the Q-switch and aperture simultaneously.

Wavelength scans were performed on I_2/Ar mixtures, taking advantage of the photolysis of I_2 at 266 nm previously noted. The delay between the two lasers was fixed at the time of largest signal for a 293 K saturated vapor pressure of I_2. The wavelength of the probe laser was then scanned to obtain a spectrum.

B. Materials. Iodine (Fischer, Reagent Grade) was vacuum sublimed at 293 K into a 77 K cold finger which could be attached to the LIF cell. The I_2 concentration could be varied and maintained from approximately 30 to 300 mtorr by the use of constant temperature baths (273–293 K). Trifluoromethyl iodide (PCR, Inc.) was vacuum distilled from 175 to 158 K and then subjected to several freeze–pump–thaw cycles. It was expanded into the cell from a reservoir at 158 K at the time of use. Argon (Matheson, 99.9995%) was withdrawn from a bulb held at 77 K for expansion into the cell.

III. Kinetic Models

Several kinetic models at various levels of complexity are used in the interpretation of the results to be presented in section IV. The simplest model considers only the reactions

$$I^* + I_2 \rightarrow I(v{=}40) + I \qquad (1c)$$

$$I_2(v{=}40) + M \rightarrow I_2(v{<}40) + M \qquad (8)$$

This model is of the

$$A \xrightarrow{k_B} B \xrightarrow{k_C} C$$

type, for which the time dependence of B, following a rapid initial creation of A in concentration A_0, is given by the sum of a rising and falling exponential:[30]

$$B(t) = \frac{k_B A_0}{k_C - k_B}(e^{-k_B t} - e^{-k_C t}) \qquad (9)$$

It should be noted that if $k_B > k_C$, i.e., if the formation of B is faster than its decay, then k_B will be the observed rise rate. On the other hand, if $k_C > k_B$, then the observed rise rate is k_C, the rate at which B is destroyed. In the present case, relaxation of vibrationally excited I_2 is always faster than I* quenching by I_2, so that the experimentally observed rise rate is associated with the vibrational relaxation and the fall rate with the quenching of I* by I_2. Experimental verification of this assertion will be presented in section IV.

When processes are included such as

$$I^* + I_2 \rightarrow I_2(v{\neq}40) + I \qquad (10)$$

which quench I* but do not populate the observed vibrational level, the model becomes

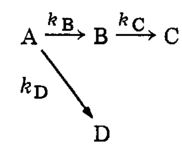

and the time dependence of B is only slightly modified:

$$B(t) = \frac{k_B A_0}{k_C - (k_B + k_D)}(e^{-(k_B+k_D)t} - e^{-k_C t}) \qquad (11)$$

A more complete kinetic scheme considers each vibrational level of I_2 separately, allowing some fraction of the total I* + I_2 quenching encounters to populate each vibrational level, and then considers the cascade of vibrational relaxation (dominated by v to $v - 1$ processes of the V–T type):

$$I^* + I_2 \xrightarrow{k_v} I + I_2(20{<}v{<}45) \qquad (1b)$$

$$I_2(20{<}v{<}45) + M \xrightarrow{k_r} I_2(19{<}v{-}1{<}44) \qquad (12)$$

where the known total quenching rate of I* by I_2 is given by

$$\sum_{v=0}^{45} k_v = k_{1c} + k_{10} \qquad (13)$$

A simple computer program was used to model this kinetic system. It was assumed for simplicity that k_r was independent of v. The relative values of k_v, i.e., the distribution of I_2 vibrational states directly populated by energy transfer, and k_r were treated as unknowns and independently varied over a reasonable range of expectations.

Qualitatively, one should expect (and finds) that the time dependence of the population in a vibrational level will show simple rise and fall kinetics (differences of exponentials) if the contribution to the population due to direct formation far exceeds the contribution due to cascading from higher vibrational levels. Conversely, if the dominant portion of the population passing through a vibrational level is due to cascading from higher levels, an induction time should be observed, increasing in magnitude with the difference in quantum number between the monitored level and the levels of largest direct population. One could thus use the variations in the observed kinetics at different levels to infer the gross features of the vibra-

(30) G. G. Hammes, "Principles of Chemical Kinetics", Academic Press, New York, 1978, p 10.

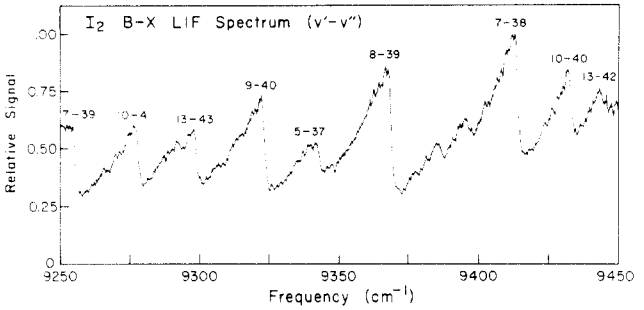

Figure 3. LIF spectrum of vibrationally hot $I_2(X)$. The conditions were as follows: 208 mtorr of I_2, 1.00 torr of Ar, and a 2.5-μs delay between the I_2 photodissociation pulse at 475 nm and the near-infrared probe pulse. Prominent bandheads are labeled.

tional distribution. This point will be discussed further in section V.B.

IV. Results

A. Spectral Identification. The fluorescence signal observed in response to the probe laser can be identified unambiguously as having originated from vibrationally excited $I_2(X)$. If either the photolysis or probe laser beam is blocked, the signal disappears, as it does when the cell is evacuated. Furthermore, the fluorescence lifetimes match reported $I_2(B-X)$ lifetimes[31] reasonably well. Most importantly, the laser-induced fluorescence spectrum obtained by scanning the probe laser in the 900–1100-nm region displays bandheads which accurately coincide with the calculated positions of B–X vibronic bands originating in the levels $25 < v < 43$. A typical scan of 200 cm^{-1} in the near-infrared is shown in Figure 3. Individual rotational lines are not resolved in this scan since there are approximately 50 lines/cm^{-1} and the laser line width is about 0.5 cm^{-1}. The rotational contours correspond to room temperature rotational distributions. This observation is reasonable since the spectrum was taken in the presence of 1 torr of argon under conditions where rotational relaxation is expected to be fast compared to the vibrational lifetime. From all the observed spectra it is evident that a broad distribution of vibrational levels is populated, either directly or by cascading, or both. More detailed information about the distribution and its kinetics can be obtained by tuning the probe laser to an isolated bandhead and scanning the delay between the photolysis and probe lasers.

B. Kinetics at $v = 40$. Since the 9–40 band is well isolated from overlapping bands, 9318 cm^{-1} was chosen as the probe frequency for monitoring the kinetics of $I_2(v=40)$. Scanning the delay between the photolysis laser which created the I* and the probe laser which monitored $I_2(v=40)$ resulted in data typified by Figure 4a. The time dependence is well represented by a difference of exponentials; the solid line is a least-squares fit to eq 11. The rates derived from such time scans for samples with varying amounts of I_2 in 1 torr of Ar are shown in parts a and b of Figure 5 for the rise and decay, respectively. At a fixed I_2 pressure of 25 mtorr, the effects of varying the Ar pressure on the rise and fall rates is shown in Figure 6. These first-order plots give second-order rate constants of $(1.8 \pm 0.4) \times 10^6$ and $(1.0 \pm 0.1) \times 10^6$ s^{-1} $torr^{-1}$ for the rise and decay, respectively, when I_2 was varied. For the variation of Ar pressures, a second-order rate constant of $(7.3 \pm 0.3) \times 10^5$ s^{-1} $torr^{-1}$ was obtained for the rise, while no dependence on Ar pressure was found for the decay.

(31) K. Sakurai, G. Capelle, and H. Broida, *J. Chem. Phys.*, 54, 1220 (1971).

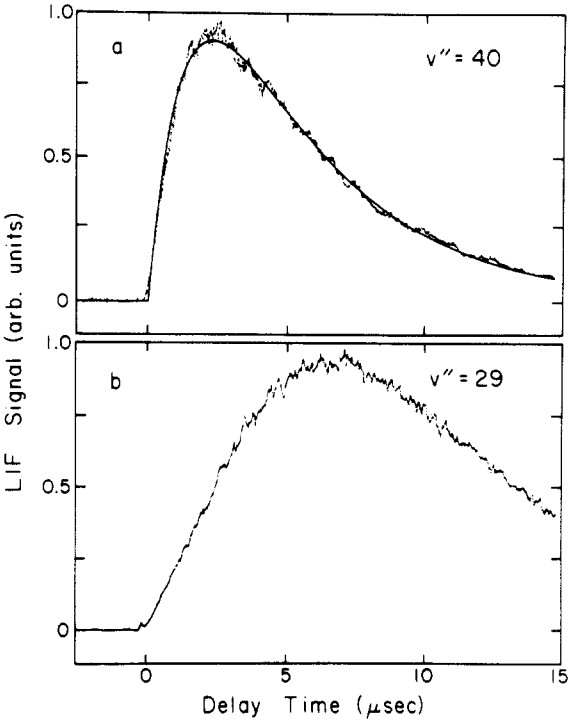

Figure 4. Time dependence of selected vibrational levels of $I_2(X)$ following I* formation. (a) The probe laser was tuned to 9318 cm^{-1} where the dominant contribution is from $v'' = 40$. (b) The probe laser was tuned to 11 664 cm^{-1} where the dominant contribution is from $v'' = 29$. Conditions for both measurements were as follows: 30 mtorr of CF_3I, 200 mtorr of I_2, 1 torr of Ar, and photodissociation at 266 nm.

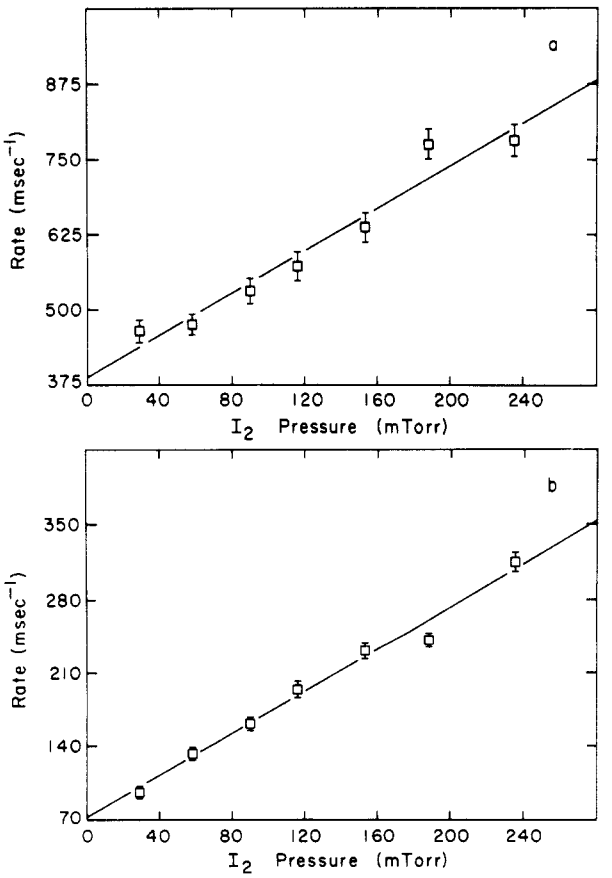

Figure 5. I_2 pressure dependence of rise (a) and fall (b) rates observed for $I_2(v=40)$. The Ar pressure was fixed at 1.0 torr, the CF_3I pressure was fixed at 30 mtorr, and the photodissociation was at 266 nm. The slope of the rise rates vs. I_2 pressure is $(1.8 \pm 0.4) \times 10^6$ s^{-1} $torr^{-1}$. For the fall rates the slope is $(1.0 \pm 0.1) \times 10^6$ s^{-1} $torr^{-1}$.

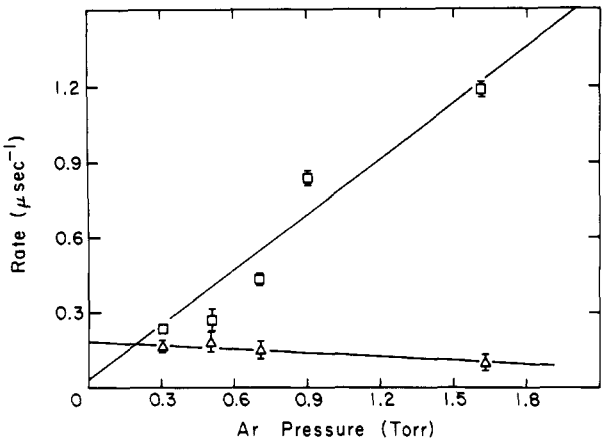

Figure 6. Argon pressure dependence of rise (squares) and fall (triangles) rates observed for $I_2(v=40)$. The I_2 pressure was fixed at 25 mtorr, the CF_3I pressure was fixed at 30 mtorr, and the photodissociation was at 266 nm. The slope of the rise rates vs. Ar pressure is $(7.3 \pm 0.3) \times 10^5$ s^{-1} $torr^{-1}$. For the fall rates the slope is $(-3 \pm 4) \times 10^4$ s^{-1} $torr^{-1}$.

When He was substituted for Ar and its pressure varied in a similar manner, a rate constant of $(1.0 \pm 0.2) \times 10^6$ s^{-1} $torr^{-1}$ was measured for the rise, while the decay rate was again independent of He pressure. In all cases except at low pressures of buffer gas, good fits to differences of exponentials were obtained. When the buffer gas pressure is too low, the analysis of the kinetics is complicated by the need to account for diffusion out of the probe volume of the cell.

C. Kinetics at v = 29. The 14–29 band is also well isolated from overlapping bands, so the probe laser was tuned to this bandhead to monitor the time dependence of $I_2(X,v=29)$. A typical time scan (Figure 4b) shows that, for similar experimental conditions, the maximum of the signal is shifted to later times compared to that for v = 40 (Figure 4a) and that it is not possible to fit the temporal profile with a difference of exponentials.

D. Calibration of LIF Sensitivity. In order to estimate the total efficiency of the E → V process relative to other possible quenching pathways, we made a calibration of the absolute sensitivity using LIF of room temperature I_2 excited with visible radiation.

A single excitation laser, tuned to the I_2 9–0 transition at 16 788.9 cm^{-1}, followed the normal path of the probe laser into the cell. It was determined from the resulting fluorescence that a fluence of 0.3 $\mu J/cm^2$ was required to induce a signal comparable to those observed in the I* + I_2 two laser experiment. This pulse energy was determined from the measured attenuation of a stack of neutral density filters and a large (mJ) pulse energy measured with a Coherent 210 power meter. This beam, as well as all the other probe and photolysis beams, was expanded to fill the $^3/_8$-in. diameter apertures of the baffles in the fluorescence cell.

The near-infrared probe laser was then reintroduced into the system (by changing dyes and adding a Raman shifter) to compare fluorescence signals excited from in v'' = 40 under nearly identical conditions. I* was produced by dissociation of I_2 at 475 nm with a fluence of 0.5 mJ/cm^2, as measured at the fluorescence cell exit window. It was found that a probe laser fluence of 1.25 mJ/cm^2 produced a signal 43% as strong as that induced by the visible laser alone. The conditions of measurement were as follows: 208 mtorr of I_2, 1.00 torr of Ar, and a 2.5-μs delay between creation of I* and probing of $I_2(v=40)$. The extraction of an E → V efficiency from these measurements will be discussed in the next section.

V. Discussion

A. Calculation of LIF Sensitivity and Estimation of E → V Efficiency. Measured laser fluences, sample pressures, and fluorescence signals were combined with calculated absorption cross sections to yield an estimate of the efficiency of vibrational excitation of I_2 by I*. The calculations are in five steps, described in detail in the subsections below. Briefly, the steps are as follows: (1) Computation of the density of $I_2(B,9<v'<13)$ present when a known LIF signal is observed. A room temperature sample of I_2 was excited by visible light at ≈596 nm for this calibration. (2) Computation of the fraction of $I_2(X,v''=40)$ that would be pumped to $I_2(B,v'=9)$ by the near-IR probe beam of measured fluence. (3) Computation of the density of $I_2(X,v''=40)$ at a specified time following the creation of I*, using the observed LIF signal and the results of calculations 1 and 2 above. (4) Computation of the density of I* formed at t = 0 by the dissociation laser. (5) Combination of the results of calculations 3 and 4 to give the fraction of I* quenching events which leads directly to $I_2(X,v''=40)$, using the measured time dependence of $I_2(X,v''=40)$ and a kinetic model.

1. Sensitivity Calibration. Exciting a sample of room temperature I_2 of a measured pressure with a laser pulse of known wavelength, line width, and fluence will populate a calculable density of excited I_2 molecules with a calculable distribution of v',J'. The strength of the subsequent B–X emission observed from such an excited sample can be compared to the emission observed following the near-infrared probe of vibrationally hot I_2.

Absorption coefficients for individual rotational lines of the B–X transition in I_2 were computed by techniques similar to those described by Tellinghuisen.[32] Spectroscopic constants for the X and B states[33,34] of I_2 were incorporated into a program that identified all B–X rotational lines in a specified energy range. For the orange light chosen for this calibration, 16 788.9 cm^{-1}, there are about 100 lines from about 10 different vibronic bands within $\pm 3\sigma$ of the center laser frequency. For each rotational line, the absorption coefficient, $k(\nu)$ (cm^{-1}), is approximately given by

$$\int_0^\infty k(\nu)\, d\nu = \frac{8\pi^3\nu}{3hc}\, \mu_e^2(\bar{R})|\langle v'|v''\rangle|^2\, \frac{S_{J'J''}}{2J''+1} f_{ns} N(v'',J'') \tag{14}$$

where ν is the wavenumber (cm^{-1}), h is Planck's constant, c is the speed of light, and $\mu_e(\bar{R})$ is the average electronic transition moment, a function of the $\bar{R}$-centroid $\langle v'|R|v''\rangle/\langle v'|v''\rangle$. The squared matrix element is the Franck–Condon factor, $S_{J'J''}$ is the rotational line strength, f_{ns} is a nuclear spin degeneracy factor ($^5/_6$ for even J'', $^7/_6$ for odd J'') and $N(v'',J'')$ is the number density of absorbing molecules in the level (v'',J''). In this case, $N(v'',J'')$ was given by the thermal distribution of eq 15. Here N_0 is the

$$N(v'',J'') = N_0(2J''+1)\frac{hcB_e}{kTQ_V} \exp(-E(v'',J'')/kT) \tag{15}$$

total number density of I_2, B_e is the rotational constant, k is the Boltzmann constant, Q_V is the vibrational partition function, $\sum_{v''=0}^{\infty} e^{-E(v'')/kT}$, and $E(v'',J'')$ is the energy of the (v'',J'') level relative to the 0,0 level.

The Franck–Condon factors and R centroids were calculated by standard techniques.[35] RKR turning points

(32) J. Tellinghuisen, *J. Chem. Phys.*, **76**, 4736 (1982).
(33) J. Tellinghuisen, M. R. McKeever, and A. Sur, *J. Mol. Spectrosc.*, **82**, 225 (1980).
(34) P. Luc, *J. Mol. Spectrosc.*, **80**, 41 (1980).

for X and B state potentials were computed from spectroscopic constants; interpolation with a seven-term polynomial gave a table of $V(R)$ for both potentials. Vibrational wave functions were computed for these potentials by the Numerov–Cooley[36] solution to the Schroedinger equation, and finally, the Franck–Condon factors and $\bar{R}$ centroids were obtained by trapezoidal integration of the wave function products. In cases where comparison with previously published Franck–Condon factors can be made, our values typically agree within 10%. Transition moments were interpolated from the data of Koffend, Bacis, and Field[37] using our calculated $\bar{R}$ values.

Each rotational line was assumed to be Gaussian with a fwhm, $\Delta\nu$, of 0.032 cm^{-1} and a consequent peak absorption coefficient k_0 given by

$$k_0 = \frac{2}{\Delta\nu}\left(\frac{\ln 2}{\pi}\right)^{1/2}\int_0^\infty k(\nu)\,d\nu \tag{16}$$

The lines are broadened by a combination of Doppler and hyperfine structure. The result is not Gaussian, but, since the laser line width is almost 20 times greater than the absorption line widths, the use of the average measured widths and Gaussian profiles is adequate. Thus, for the ith rotational line considered, we compute the contribution to the absorption at wavenumber ν as

$$k_i(\nu) = k_{0i}\exp\left(-\left[\frac{2(\ln 2)^{1/2}(\nu-\nu_{0i})}{\Delta\nu}\right]^2\right) \tag{17}$$

The total absorption coefficient at ν, k_ν, is the sum of contributions from all nearby lines:

$$k_\nu = \sum_i k_i(\nu) \tag{18}$$

The fraction of light absorbed at wavenumber ν in 1 cm of optical path in the region viewed by the detector (32 cm inside the cell) is

$$\text{absorbed fraction/cm} = e^{-k_\nu\cdot 32}(1 - e^{-k_\nu\cdot 1}) \tag{19}$$

For a laser beam with a Gaussian frequency distribution, $I(\nu)$, the total density of excited states in front of the detector is

$$N_{I_2(B)} = \int_0^\infty I(\nu)\,e^{-k_\nu\cdot 32}(1 - e^{-k_\nu})\,d\nu \tag{20}$$

where $I(\nu)$ is expressed in photons/(cm^2 pulse cm^{-1}), and the total fluence I_0, in photons/(cm^2 pulse), is given by

$$I_0 = \int_0^\infty I(\nu)\,d\nu \tag{21}$$

In the optically thin limit ($k_0 << 1$ cm^{-1}), eq 20 can be linearized to

$$N_{I_2(B)} = \int_0^\infty I(\nu)k_\nu\,d\nu \tag{22}$$

In the present case, however, several lines in this spectral region absorb as much as 40% of the light at their frequencies of maximum absorption, so that the more general eq 20 is required.

We calculate from eq 20 that 3.3×10^{-3} of the total fluence is absorbed per centimeter in the middle of the cell. Thus, for an incident 596-nm probe fluence of 0.3 $\mu J/cm^2$, a density of 3.2×10^9 molecules/cm^3 of I_2(B) is created.

The distribution of v' levels in the B state was calculated by tallying the individual contributions from each vibronic band to the total excitation calculated in eq 20. The dominant v' levels were 13, 11, 12, and 9 with respectively 46, 29, 14, and 3% of the total B state population. The observed LIF signal from 3.2×10^9 molecules/cm^3 with this v' distribution was 0.87 full scale. To compare this with a LIF signal later to be detected from a distribution which is predominantly $v' = 9$, we must correct for the v' dependent detection efficiency. The detection efficiency may vary with the fluorescence quantum yield and with the fraction of the fluorescence spectrum of each v' level that is accepted by the optical band-pass filter of the detection system, 600 nm $< \lambda <$ 650 nm. The spectral overlap corrections were estimated by summing the Franck–Condon factors for each v' level of the bands (v',v'') which had origins in the detected spectral region. The fluorescence quantum yield corrections were negligible. Applying those corrections, we estimate that, if the I_2(B) molecules were all in $v' = 9$ instead of in the actual distribution of v' levels, the observed signal would have been larger by 32%. We thus conclude that a full scale signal on our LIF detection system would be observed from a population of 2.8×10^9 molecules/cm^3 of I_2(B,v'=9).

2. Near-Infrared Pumping Efficiency. Absorption cross sections for B–X rotational lines in the vicinity of the (9,40) bandhead at 9318 cm^{-1} were computed as in section V.A.1. Since the populations $N(v'',J'')$ were not initially known, the absorption strengths were expressed as cross sections, σ_0.

$$\sigma_0(v'',J'') = \frac{k_0}{N(v'',J'')} \tag{23}$$

The fractional excitation of a level (v'',J'') in the low-intensity limit is

$$\frac{\Delta N}{N(v'',J'')} \simeq \int_0^\infty \sigma_0 \exp\left[-\left(\frac{2(\ln 2)^{1/2}(\nu-\nu_0)}{\Delta\nu}\right)^2\right] I(\nu)\,d\nu \equiv \langle I\sigma\rangle_{v'',J''} \tag{24}$$

At high intensities ($\langle I\sigma\rangle_{v'',J''}$ not $<< 1$), optical saturation of two levels of nearly equal degeneracies [$2J'' + 1$ vs. ($2J'' + 1$) ± 2] that have negligible relaxation during the 5-ns excitation pulse is adequately represented by

$$\frac{\Delta N}{N(v'',J'')} = \frac{1 - \exp[-2\langle I\sigma\rangle_{v'',J''}]}{2} \tag{25}$$

This equation has the correct low- and high-intensity limits of $\langle I\sigma\rangle_{v'',J''}$ and 1/2, respectively.

The fractional excitation of each vibrational level v'' was computed according to (26), assuming a room temperature

$$\frac{\Delta N}{N(v')} = \sum_{J''}(2J'' + 1)\frac{hcB}{kT}\exp[-E_{J''}/kT]\left(\frac{1 - \exp[-2\langle I\sigma\rangle_{v'',J''}]}{2}\right) \tag{26}$$

rotational distribution for each vibrational level. The sum over J'' can be seen to include nonzero contributions only for the rotational lines of the (v'',v') band which are close to the laser frequency. About 80 rotational lines were found within $\pm 3\sigma$ of the laser frequency originating in $33 \le v'' \le 43$ and $0 \le J'' \le 150$. About half of these lines were from the (9,40) vibronic band.

The fractional excitation of v'' levels from 33 to 43 was computed from eq 26. We find that the near-infrared

(35) R. N. Zare, *J. Chem. Phys.*, **40**, 1934 (1964).
(36) J. Eccles and D. Malik, *QCPE*, **13**, 407 (1981).
(37) J. B. Koffend, R. Bacis, and R. W. Field, *J. Chem. Phys.*, **70**, 2366 (1979).

probe should excite 3.7% of the total $v'' = 40$ population to $I_2(B,v'=9)$. Only $v'' = 39$ and 37 are also significantly excited, to the extent of 0.6 and 0.5%, respectively.

3. Population of $I_2(X,v''=40)$ at $t = 2.5$ μs. The observation of a 0.35 full scale signal following the near-infrared probe delayed 2.5 μs from the I_2 dissociation laser indicates a density of 9.8×10^8 molecules/cm^3 that are detected with the same efficiency as $I_2(B,v'=9)$. If we assume equal concentrations of $I_2(X,v'')$ for $37 \leq v'' < 43$ (as seems plausible from our LIF scans) the calculations of section VA.2 indicate that 70% of all excitation is to $v' = 9$ from $v'' = 40$. Most of the rest of the excitation is to $v' = 8$ and 5 from $v'' = 39$ and 37, respectively. After applying small corrections for the detection efficiencies of these other v' levels, we conclude that a density of 1.8×10^{10} molecules/cm^3 in each of the vibrational levels near $v = 40$ would result in a LIF signal of the amplitude we observed.

4. I Density from Photodissociation of I_2.* When excited above its dissociation threshold, $I_2(B)$ gives I* + I with a quantum yield of 1.0. The extinction coefficient for the B–X portion of the continuum absorption (the 1u–X portion does not give I*) at 475 nm interpolated from Tellinghuisen's data is $\epsilon_{475} = 133$ M^{-1} cm^{-1}. In molecular units, this is $\sigma_{B-X} = 5.1 \times 10^{-19}$ cm^2/mol. The total extinction coefficient at 475 nm is 270 M^{-1} cm^{-1} which implies 64% transmission of this light through our sample, comparable to our measurements. The transmitted fluence was 1.0×10^{15} photons/cm^2 and the fluence at the detection region, I(32 cm), was thus 1.25×10^{15} photons/cm^2. The density of I* calculated from eq 27 was 4.3×10^{12} atoms/cm^3.

$$N_{I^*} = N_{I_2}\sigma_{B-X}(475\text{ nm})I(32\text{ cm}) \quad (27)$$

5. Kinetic Analysis to Give E → V Efficiency. We consider the time dependence of $I_2(X,v''=40)$ to be consistent with the kinetic model described earlier.

$$I^* + I_2 \xrightarrow{k_{1c}} I + I_2(v''=40) \quad (1c)$$

$$I^* + I_2 \xrightarrow{k_{10}} I + I_2(v''\neq 40) \quad (10)$$

$$I_2(v=40) + M \xrightarrow{k_8} I_2(v''\neq 40) + M \quad (8)$$

When $[I_2] >> [I^*]$, the solution for $I_2(v''=40)$ is

$$I_2(v''=40)_t = I^*_{t=0}\frac{k_{1c}[I_2]}{k_8[M] - ((k_{1c} + k_{10})[I_2])}\{e^{-(k_{1c}+k_{10})[I_2]t} - e^{-k_8[M]t}\} \quad (28)$$

The observed time dependence of the LIF signal on the 9–40 bandhead was shown in Figure 4a, and the fit to a difference of exponentials is good. The rise rate of 0.78 ± 0.04 μs^{-1} is k_8[M] and the fall rate of 0.22 ± 0.01 μs^{-1} is $(k_{1c} + k_{10})$[I_2]. The $I_2(v''=40)$ concentration was determined at $t = 2.5$ μs, so eq 28 has a single unknown: k_{1c}[I_2]. Its value is 5.4×10^{-3} μs^{-1} at this I_2 pressure and the ratio $k_{1c}/(k_{1c}+k_{10}) = 0.024$. This is the fraction of I* quenched by I_2 which directly populates $I_2(X,v''=40)$. When combined with similar fractions in other high vibrational levels, it is evident that this E → V process may be a dominant part of the I* quenching by I_2.

B. The Vibrational Distribution of I_2. The exact distribution of I_2 vibrational levels populated by energy transfer is difficult to determine from the relative intensities of the LIF bands. The relative intensities can give relative populations *at a specified time*, but, since the time dependence of each level is different and reflects a combination of direct and indirect formation, the direct formation rates into each level cannot be simply determined. Only at the highest levels populated, where indirect formation from still higher levels can be neglected, can a reasonably quantitative analysis be performed, as in the previous section.

A qualitative estimate of the vibrational distribution can be obtained from the observed time dependence of several levels when compared with the model calculations for the multilevel system described in section III. If a statistical distribution is assumed, as if originating from the unimolecular decomposition of a long-lived (I* + I_2) complex, the probability that the I_2 will be ejected with quantum number v is proportional to $(1 - f_v)^{3/2}$, where f_v is the fraction of the I* energy that appears as vibrational energy.[38] This probability is a monotonically decreasing function of v, and the probability of formation with $v >$ 25 is about 8%. The time dependence determined from the model calculations for levels $v > 25$ can be well represented by a difference of exponentials, with the rise rates decreasing with lower v. The downward curvature at early times predicted by the model calculations is not in agreement with the nearly linear rise in the $v = 29$ data of Figure 4b, although the position of the maximum and rate of subsequent decay are approximately correct. A second result inconsistent with the statistical distribution is the estimated efficiency of population of $I_2(v=40)$ from I* + I_2 quenching. The value derived in section VA of about 2% is much too high to be a part of the statistical distribution, for which the population decreases very rapidly at high v.

Other vibrational distributions were considered, looking for those which were consistent with the observed shape of the time dependence of $I_2(v=29)$ and $I_2(v=40)$. Any noninverted population distribution showed downward curvature for $v = 29$, contrary to observation. Population distributions sharply peaked near $v = 40$ showed flat induction times followed by a rise with upward curvature at early times for $v = 29$, also contrary to observation. So that the data of Figure 4 could be reproduced, an inverted population distribution is required such that the population of $v = 29$ is formed predominantly by cascading from higher levels, but also with some significant direct formation. Many such distributions are possible, even more so when the possibility of level-dependent vibrational relaxation rates or multiquantum deactivations is allowed. The experimental measurements are insufficient to draw quantitative conclusions from such methods. However, it does seem safe to conclude that the nascent vibrational distribution of I_2 is inverted, with a substantial fraction having $v > 30$.

The conclusions described in this section about the approximate I_2 vibrational distribution can be combined with the calculation described in section VA of 2% for the E → V efficiency for $v = 40$ in order to estimate the total efficiency of E → V transfer from I* to I_2. Given the uncertainties in the calibration method and in the determination of the distribution, we would not be surprised if the total E → V efficiency were as high as 100% or as low as 15%, but the E → V channel is definitely not a negligible deactivation pathway.

C. The Mechanism of E → V Transfer from I to I_2.* In most previously studied cases of E → V transfer from excited halogen atoms,[1] deactivation appears to proceed predominantly through near resonant energy transfer of the type

$$X^* + AB(v') \rightarrow X + AB(v) + \Delta E$$

(38) D. J. Bogan and D. W. Setser, *J. Chem. Phys.*, 64, 586 (1976).

where ΔE, the amount of energy which must be taken up by translation and rotation, is found to be a minimum. From this point of view it is not surprising that the current study has observed high vibrational excitation of I_2 with at least some direct population of $v = 40$, the I_2 level in near resonance with the electronic energy of I*. On the other hand, the total deactivation rate of I* by I_2 seems to be higher than one would expect. In previous studies it has been observed that, given the same ΔE, higher total deactivation rates are observed when $\Delta v = v' - v''$ is a minimum. The I^*/I_2 system seems to be an exception to this rule since the total rate of I* deactivation by I_2, where $\Delta v = 40$ is required for $\Delta E \approx 0$, is about 100 times faster than the rate of I* deactivation by HD, where $\Delta E \approx 0$ and Δv is only 2. It is thus somewhat difficult to explain why the I^*/I_2 system has *both* a high total deactivation rate and a relaxation dominated by resonant E → V energy transfer. It seems likely that a bound I_3^* complex is responsible. The existence of the stable ground state of I_3 has been inferred from measurements of the rate of iodine atom recombination,[39] and a stable linear state of Cl_3 has been observed in cryogenic matrices by Nelson and Pimentel.[40] However, nothing is known about the electronically excited states of either I_3 or Cl_3. One hypothesis which might explain the results observed in this study is that I* and I_2 form a bound I_3^* complex which is then dissociated by crossing to curves leading to $I + I_2(v)$. Further understanding of the mechanism of this E → V transfer will require more information about the I_3 molecule.

D. Relevance of These Observations to the Chemical Oxygen/Iodine Laser. The mechanism of I_2 dissociation in the chemical oxygen/iodine laser has recently become a center of controversy. Results from our own laboratory[11,12] have shown that while the steps

$$O_2(^1\Delta) + O_2(^1\Delta) \rightarrow O_2(^1\Sigma) + O_2(^3\Sigma) \quad (2)$$

$$O_2(^1\Sigma) + I_2 \rightarrow O_2(^3\Sigma) + 2I \quad (4)$$

occur, the rate constant for reaction 4 is less than about 4×10^{-12} cm^3/(molecule s). This rate is far too slow to account for the rapid disappearance of I_2 in the flow-tube experiments of Heidner et al.[13] In a more recent paper, Heidner et al. have provided evidence for a chain-branching mechanism in which an excited I_2 intermediate, $I_2^\ddagger$, is created by energy transfer from I* and is then dissociated by collision with either $O_2(^1\Delta)$ or I*.[41] The main evidence for this mechanism is the observation that the half-life for I_2 dissociation becomes *shorter* as the initial concentration of I_2 is increased. Initiation of the proposed chain branching reaction was thought to occur either by the sequence of reactions 2–4 or by reaction of free oxygen atoms with I_2. Termination was shown to occur by recombination of iodine atoms on the walls of the flow tube. However, the identity of $I_2^\ddagger$ was not resolved. The excited I_2 intermediate was thought either to be the $I_2(A'\,^3\Pi_{2u})$ state, as first suggested by Ogryzlo and his co-workers,[2] or to be vibrationally excited I_2, as suggested by ourselves and others.[42,43] The former suggestion has since been discounted by recent spectroscopic measurements.[44,45] The direct observation of electronic-to-vibrational energy transfer from I* to I_2 reported in this paper strongly supports the latter identification.

Nonetheless, serious questions remain concerning the assignment of the $I_2^\ddagger$ in the proposed chain-branching mechanism to the vibrationally excited I_2 observed in this work. In combination with their model of the dissociation, the observation by Heidner et al.[41] that the I_2 half-life varies as $[O_2(^1\Delta)]^{-2}$ suggests that, if dissociation of $I_2^\ddagger$ occurs via energy transfer from $O_2(^1\Delta)$, then deactivation of the intermediate must compete effectively with dissociation. Furthermore, the observed insensitivity of the I_2 half-life to argon pressure forced these authors to conclude that the rate of deactivation of $I_2^\ddagger$ by oxygen must be about 12–500 times greater than the rate of deactivation by argon. Our measurements of the rate of $I_2(v=40)$ deactivation by argon is about 7.3×10^5 s^{-1} torr^{-1}, so that the model of Heidner et al. would require the rate of deactivation by O_2, as well as the rate of dissociation by $O_2(^1\Delta)$, to be 1–25 times gas kinetic. Consequently, if $I_2^\ddagger$ is taken to be the single level $I_2(v=40)$, the comparison of our data with that of Heidner et al. leaves doubt as to the viability of the chain-branching mechanism. However, dissociation by $O_2(^1\Delta)$ of any level with $20 < v < 40$ is energetically allowed. Since all the levels have different time dependences, treating them together as a single intermediate with first-order rate constants for formation and destruction is probably unjustified. If vibrational relaxation occurs primarily by $v \rightarrow v - 1$ processes, then the time required for deactivation to levels with $v < 20$ will be considerably longer than the lifetime implied by the deactivation rate constant for $v = 40$. Thus the detailed kinetics of the $I_2(v)$ distribution may explain both why the I_2 dissociation half-life is insensitive to argon pressure and how the dissociation of $I_2(v)$ by $O_2(^1\Delta)$ can compete with deactivation.

VI. Conclusion

Electronic-to-vibrational energy transfer from I* to $I_2(25<v<43)$ has been directly observed. It is likely from our results that the E → V channel is a major deactivation pathway. About 2% of the I* deactivations produce $I_2(v=40)$. The experimental results are consistent with a nascent I_2 product distribution which is inverted, with a substantial fraction of the I_2 molecules formed in $v > 30$. The rate constants for vibrational relaxation of $I_2(v=40)$ by argon, helium, and I_2 at room temperature are $(7.3 \pm 0.3) \times 10^5$, $(1.0 \pm 0.2) \times 10^6$, and $(1.8 \pm 0.4) \times 10^6$ s^{-1} torr^{-1}, respectively. Much work must be done to understand theoretically the mechanism for the E → V process. The nature of the I_3 potential energy surfaces and the magnitude of the coupling between them need to be determined.

These results have important implications for the mechanism of I_2 dissociation in the chemical oxygen/iodine laser. A chain-branching mechanism consisting of the steps $I^* + I_2 \rightarrow I + I_2(20<v<40)$, $I_2(20<v<40) + O_2(^1\Delta) \rightarrow 2I + O_2$, and $O_2(^1\Delta) + I \rightarrow O_2 + I^*$ may be responsible for the dissociation. However, much more work must be done before this mechanism can be assigned with certainty. Vibrational deactivation rates for I_2 levels from $v = 20$ to $v = 40$ must be measured, and the rates for dissociation of these levels by $O_2(^1\Delta)$ must be determined. Any complete model of the dissociation must take into account the distribution of population among the vibrational levels and the cascading of energy down the vibrational ladder.

Acknowledgment. We are very grateful to J. Tellinghuisen for making available his RKR program, to R. F. Heidner III for providing us with a preprint of ref 41, and to R. F. Heidner III, J. R. Wiesenfeld, E. R. Grant, and

(39) D. L. Bunker and N. Davidson, *J. Am. Chem. Soc.*, **80**, 5090 (1958).
(40) L. Y. Nelson and G. C. Pimentel, *J. Chem. Phys.*, **47**, 3671 (1967).
(41) R. F. Heidner III, C. E. Gardner, G. I. Segal, and T. M. El-Sayed, *J. Phys. Chem.*, to be published.
(42) R. F. Heidner III, private communication, 1981.
(43) Citations 20 and 21 in ref 41.
(44) J. Tellinghuisen and K. Wieland, *J. Mol. Spectrosc.*, to be published.
(45) J. B. Koeffend, R. Bacis, and A. Sebai, to be published.

H. Michels for helpful discussions. This work was supported by AFOSR under Grant No. 78-3513. The experiments were performed in the Facility for Laser Spectroscopy in the Chemistry Department of Cornell University. The capital equipment in this facility was provided in part by a grant from the National Science Foundation Instrumentation Program.

Registry No. Iodine, 7553-56-2; atomic iodine, 14362-44-8; trifluoroiodomethane, 2314-97-8; argon, 7440-37-1; helium, 7440-59-7.

Dynamical Symmetry Breaking and Energy Transfer Pathways in Local Modes of Benzene

Michael E. Kellman

Department of Chemistry, Northeastern University, Boston, Massachusetts 02115 *(Received: November 29, 1982)*

Local modes are discussed as a manifestation of dynamical symmetry breaking. For benzene C–H fundamentals, the symmetry is lowered from D_{6h} to C_{2v} when the excitation process singles out one of the local modes. The "paradox" of symmetry breaking is removed, however, when one takes into account "dynamical tunneling" mechanisms which restore D_{6h} symmetry through energy transfer among the local modes. The situation is related to permutation-inversion isomerism in molecules with identical nuclei, with restoration of full permutation-inversion symmetry by means of tunneling among the isomers. It is shown that mathematically, the analogy subsists in the treatment of both cases in terms of induced and subduced representations and the Frobenius reciprocity theorem. It is then shown how local modes symmetry breaking may be incorporated within the framework of fundamental permutation-inversion symmetry. Splittings in local modes spectra are parameterized phenomenologically by classifying the dynamical tunneling mechanisms, or energy transfer pathways among local modes, available to the system. The phenomenological analysis of observed spectra yields relative strengths for the various pathways. The results are compared with predictions of a recent model and with intuition.

I. Introduction

Recently, Burberry and Albrecht[1] and Reddy et al.[2] have discussed the observation of monotonically decreasing absorption strength with increasing Δv in C–H stretch local modes overtones progressions in benzene. Such a spectrum seems surprising, since group theory seems to predict,[3] with the conventional assumption of D_{6h} symmetry, that $\Delta v = 2n$ overtone transitions should be forbidden. Reddy et al. explain the anomalous absorptions by postulating that, in highly excited local modes states, the molecule "suffers dynamical symmetry lowering" so that it behaves as if its invariance group is no longer D_{6h}, and in particular no longer has a center of symmetry forbidding Δv even transitions.

Recent papers show[4,5] that one need not invoke *actual* loss of D_{6h} symmetry to account for the observed spectra. In fact, the D_{6h} local modes symmetry analysis shows[5] that the spectrum provides *direct* group theoretical evidence for the local rather than collective nature of the vibrational excitation process.

Nonetheless, the notion in ref 2 of "dynamical symmetry lowering" highlights a seemingly paradoxical aspect of symmetry. A benzene molecule in its ground vibrational state is traditionally regarded as having a potential surface with D_{6h} symmetry. Excited vibrational levels in the normal modes representation would be collective excitations transforming irreducibly under D_{6h}. Although the molecule at any given instant would not in general have a hexagonal configuration, D_{6h} would remain as the symmetry group of the vibronic Hamiltonian. Persuasive evidence[1,2,4,5] indicates, however, that, with as little as one quantum of vibrational excitation, the local modes model gives a better approximation than normal modes. Suppose, then, that one places a quantum in a single C–H bond. In the zero-order local modes model, the energy remains localized in this bond; and in classical trajectory calculations on model potential surfaces,[6,7] this in fact is precisely what is observed. Is not energy localization in a single excited bond mode manifestly an instance of breaking of the D_{6h} symmetry of the initial state?

A similar "paradox" arises in molecules with several identical nuclei. Consider three ^{16}O nuclei in an ozone molecule. These nuclei are invariant under the fundamental symmetry of permutation of identical particles. However, the isosceles triangle equilibrium geometry of ozone renders the inner nucleus permutationally inequivalent to the other two. The formal consequence of this symmetry lowering is that the C_{2v} point group of ozone contains permutation of only the outer nuclei of the molecule, and not the complete set of permutations of the nuclear framework in the fundamental permutation-inversion group $S_3 \times I$.

The resolution of both "paradoxes", of course, is that the symmetry breaking is only apparent, because processes not yet considered act to restore the broken symmetry. In the case of a C_{2v} molecule such as ozone, as emphasized long ago by Berry,[8] large amplitude tunneling motions through barriers in the potential energy surface allow the interchange of nuclei between inner and outer vertices. In the case of vibrational energy localization in a local mode, a phenomenon similar to barrier penetration allows transfer

(1) M. S. Burberry and A. C. Albrecht, *J. Chem. Phys.*, **70**, 147 (1979).
(2) K. V. Reddy, D. F. Heller, and M. J. Berry, *J. Chem. Phys.*, **76**, 2814 (1982).
(3) E. B. Wilson, J. C. Decius, and P. C. Cross, "Molecular Vibrations", Dover Publications, New York, 1980.
(4) L. Halonen, *Chem. Phys. Lett.*, **87**, 221 (1982).
(5) M. E. Kellman, *Chem. Phys. Lett.*, **94**, 331 (1983).
(6) (a) R. T. Lawton and M. S. Child, *Mol. Phys.*, **37**, 1799 (1979); (b) *ibid.*, **40**, 773 (1980).
(7) M. J. Davis and E. J. Heller, *J. Chem. Phys.*, **75**, 246 (1981).
(8) R. S. Berry, *Rev. Mod. Phys.*, **32**, 447 (1960).

0022-3654/83/2087-2161$01.50/0